


An Orthotopic Model of Metastatic Nasopharyngeal Carcinoma and Its Application in Elucidating a Therapeutic Target That Inhibits Metastasis

Genes & Cancer
2(11) 1023–1033
© The Author(s) 2011
Reprints and permission:
sagepub.com/journalsPermissions.nav
DOI: 10.1177/1947601912440878
<http://ganc.sagepub.com>


Pamela A. Smith¹, David Merritt², Leah Barr¹, and David A. Thorley-Lawson²

Submitted 08-Feb-2012; accepted 10-Feb-2012

Abstract

To define and therapeutically target mechanisms that mediate nasopharyngeal carcinoma (NPC) metastasis, we have developed a unique orthotopic xenograft mouse model that accurately recapitulates the invasive and metastatic behavior of human disease. Based on clinical and laboratory evidence that the PI3K/Akt/mTOR axis is involved in aggressive NPC tumor behavior, we chose it as a therapeutic target to test the utility of our orthotopic system for evaluating the effectiveness of a targeted treatment for metastatic NPC. Demonstrated herein, we have shown that both the development and growth of metastatic lesions are markedly reduced by the mTOR inhibitor sirolimus. Thus, this orthotopic model provides a platform to study potential therapeutics for advanced NPC and demonstrates that targeting the PI3K/Akt/mTOR pathway is a promising intervention against disseminated disease.

Keywords

nasopharyngeal carcinoma, mTOR, orthotopic xenograft, metastasis

Introduction

Nasopharyngeal carcinoma (NPC) is a serious health problem in many parts of the world. Although rare in the United States and Western Europe, it is the leading form of cancer in men between the ages of 20 and 44 years in parts of Southeast Asia¹ and is prevalent in Indonesia, North Africa, the Middle East, and among Eskimo populations as well.¹ It also represents an important form of juvenile cancer, affecting a population between the ages of 15 and 25 years in North Africa,² and represents one of the most frequent epithelial tumors of children in geographically higher risk areas.³

Current treatment protocols have resulted in good clinical outcomes if the disease is diagnosed and treated at an early stage.^{4,5} Unfortunately, metastatic NPC is refractory to treatment and carries an extremely poor prognosis. Particularly concerning is, that among head and neck cancers of epithelial origin, it is associated with the highest rate of metastasis.⁶ This can be attributed in part to the clinically occult site of primary tumor development, the fossa of Rosenmüller, which often precipitates diagnostic delays that allow the cancer to become advanced before it is detected. This highlights the need for models that are amenable to the study of metastatic NPC and adequate to test new potential therapies.

Much of the information we have about NPC has been derived from studies of well-characterized cell lines *in*

*vitro*⁷ and *in vivo* using immunocompromised mice.^{8–12} To date, most NPC xenograft studies have involved the growth of a mass of tumor cells, often subcutaneously, that do not recapitulate human disease because they remain discrete and encapsulated.^{8–10} In comparison, clinically advanced NPC is characterized by aggressive invasion with erosion and remodeling of facial and skull base cranial bones¹³ as well as distant metastasis to solid organs, most commonly bone, lung, and liver.^{14,15} To more accurately replicate advanced human disease, we have developed an orthotopic mouse xenograft model of NPC by inserting luciferase-tagged tumor cells into the nasopharyngeal region and then following patterns of growth and metastasis over time. We find that placing the tumor cells in their proper microenvironment results in tumor characteristics that more accurately recapitulate metastatic and invasive human NPC. We

Supplementary material for this article is available on the *Genes & Cancer* website at <http://ganc.sagepub.com/supplemental>.

¹Department of Hematology/Oncology, Tufts Medical Center, Boston, MA, USA

²Department of Pathology, Tufts University School of Medicine, Boston, MA, USA

Corresponding Author:

Pamela A. Smith, Department of Hematology/Oncology, Tufts Medical Center, 800 Washington Street, Boston, MA 02111 (Email: psmith3@tuftsmedicalcenter.org).

found that mTOR is key to directing the outgrowth of metastatic disease. We then used the orthotopic xenograft platform to test the feasibility of blocking its activity to inhibit both metastatic NPC dissemination and pre-established metastatic growth.

Results

Identification of the PI3K/Akt/mTOR pathway as a potential therapeutic target by comparing types II and III primary biopsy specimens. To delineate pathways relevant to NPC pathophysiology, we conducted gene array analysis of primary human tissue biopsy specimens ($n = 14$), comparing nonkeratinizing differentiated type II NPC ($n = 6$) to nonkeratinizing undifferentiated type III NPC ($n = 8$) tumors (Suppl. Fig. S1A). The differentiated description of type II lesions denotes well-defined cell margins with interconnecting cords of epithelial cells.¹⁶ In contrast, type III lesions are called undifferentiated because the epithelial cells have a more pleomorphic morphology and tend to interdigitate within the surrounding lymphoepithelium.¹⁶ By contrasting 2 closely related forms of EBV-positive NPC, we sought to isolate physiologically relevant gene expression patterns that mediate their phenotypic differences while minimizing irrelevant dissimilarities. We then subjected the gene array data to analysis by the Connectivity Map, which is a publicly available database (www.broad.mit.edu/cmap) comprising gene expression profiles obtained from multiple different cell lines in response to various drugs. This tool allowed us to probe our data set, composed of differential gene expression profiles between type II and III NPC tumors, for patterns that negatively correlate with profiles that result from treating various epithelial cell lines with specific drugs^{17,18} (see Materials and Methods). The results are summarized in Supplementary Figure S1B. We found that 3 of the top 4 drugs whose effects were most highly negatively correlated with our data set are all inhibitors of the PI3K/Akt/mTOR pathway, specifically LY-294002, Wortmanin (PI3K inhibitors), and sirolimus (mTOR complex 1 inhibitor). This indicates that the intracellular pathways affected by these drugs are more highly activated in type III than type II NPC biopsy cells. These associations were highly significant individually ($P < 0.001$) but more so because all 3 target the same pathway. Because the PI3K/Akt/mTOR signaling pathway is strongly implicated in cancer progression and metastasis,¹⁹⁻²² our findings of differential activation of this axis in primary tumor biopsy specimens have potential clinical relevance that is worth exploration.

A mouse model of invasive/metastatic NPC. To explore the role of the PI3K axis in NPC tumor development and metastatic progression, we developed an orthotopic xenograft

mouse model of NPC. We tagged NPC lines C666-1 and HONE-1 with luciferase and injected them into the nasopharyngeal epithelium of severely immunodeficient NOD.Cg-Prkdcscid Il2rgtm1Wjl/SzJ (NSG) mice. All experiments are described in Table 1. In the initial experiment (Table 1, experiment 1), we found that tumors could be detected by luciferase imaging at the site of injection within 2 to 3 weeks. Histological analysis of tumor specimens confirmed locally invasive tumor growth characterized by a marked propensity for bony erosion (particularly of the skull base without parenchymal brain tissue invasion), reactive bone formation, and perineural invasion, which included cranial nerve involvement (Fig. 1A-D). These are all features that are important in the pathogenesis of primary tumor growth in human NPC disease.^{23,24} Focal lymph node invasion was apparent about 20% of the time. By comparison, when we injected C666-1 and HONE-1 cells subcutaneously (Table 1, experiment 2), we found that the tumors remained encapsulated and contained at the site of injection, showing no signs of invasiveness after 8 weeks of growth (Suppl. Fig. S2A-C). Thus, orthotopic placement of both cell lines results in formation of locally invasive tumors that model the pathological features of primary tumor growth in human NPC disease and is therefore valuable for studies of the pathogenesis of invasive NPC.

We also observed metastatic dissemination in mice injected with C666-1 cells in a distribution pattern remarkably similar to that seen in human NPC¹⁵ (Table 1), with the majority occurring in the bone, followed by the lung, and the balance distributed in the abdomen including the liver, colon, kidney, ovary, peritoneum, and adrenal gland. Figure 1 shows examples of typical metastases. In Figure 1E to 1H, tumor cells are located in the bone marrow compartment and have also infiltrated into the bony matrix of the distal femur. Figure 1I and 1J demonstrate aggressive features of bony and perineural invasion in a spinal metastasis. Metastatic lesions were also frequently found in the lung and liver, examples of which are shown in Figure 1K and 1L.

To control for the possibility that metastases arise in the C666-1-injected mice by spillover into the bloodstream during tumor cell inoculation, we performed tail vein injections in 8 mice. We intentionally used a much larger number of cells than would be expected to enter the circulation by inadvertent intravascular injections from the nasopharyngeal site. The mice were imaged weekly over 12 weeks with no evidence of tumor growth, nor was any found on dissection ($P < 0.001$ when calculated using the total of 50 mice injected orthotopically with C666-1 cells) (Table 1, experiment 2). Thus, our orthotopic model also recapitulates features of metastatic human NPC disease that arise from primary tumor growth and is therefore valuable for further studies of the pathogenesis of metastatic NPC and its therapeutic vulnerabilities.

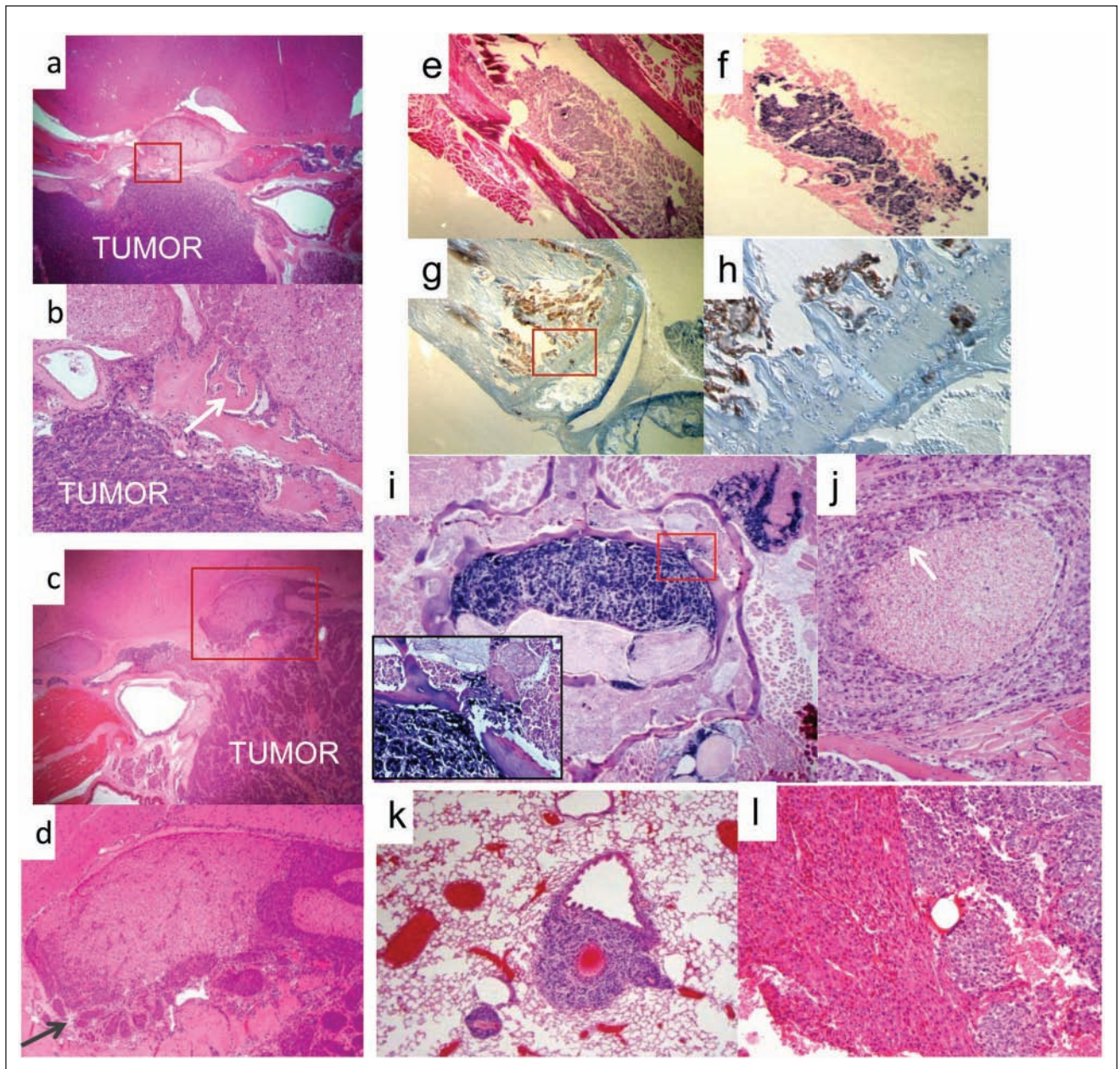


Figure 1. Histology of primary site and metastatic tumors. **(A, B)** H&E staining shows C666-1 tumor growth at the primary site of injection. The tumor has obliterated normal musculature and bony structures. A close-up view, boxed in **B**, demonstrates invasion into the base of the skull with bone destruction and reactive bone formation (indicated by white arrow). Perineural invasion is also evident, involving the trigeminal nerve. **(C, D)** H&E staining shows HONE-1 tumor growth at the primary site of injection. The tumor has obliterated normal musculature and bony structures. A close-up view, boxed in **D**, demonstrates perineural invasion of the trigeminal nerve (indicated by dark arrow). Bone destruction and reactive bone formation at the base of the skull are also seen. **(E, F)** The origin of the tumor mass in the femoral shaft of the mouse from **A**, shown by H&E stain, was confirmed through positive staining for the small EBV-encoded EBER1 RNA (**B**). **(G, H)** Pancytokeratin staining of the metastasis from **A**, demonstrating its highly invasive nature. Note the presence of tumor cells (in brown) invading and crossing the distal tibia. Pictured in **D** is a higher power view of the area boxed in **C**. **(I, J)** A spinal metastatic tumor lesion. In **E** is a low magnification view of a preparation stained for EBER1. It shows extensive tumor growth in the spinal canal as well as invasion into surrounding structures including bone (white arrow, enlarged in box), skeletal muscle, and a nearby nerve root. In **F** is an H&E preparation, showing perineural invasion of a paraspinal nerve (indicated by white arrow). **(K)** H&E preparation of a metastatic tumor in the lung. **(L)** H&E preparation of a metastatic tumor in the liver.

Table 1. Summary of Observed Rates and Sites of Metastasis

Experiment	Cell type	Injection site	No. injected/no. with 1 ⁰ tumor ^a	No. with metastases	Organ involved, with comment ^b
1	HONE-1	Nasopharynx	4/4	0	
	C666-1	Nasopharynx	8/7	3	Bone (2), ovary
2	HONE-1	Subcutaneous	7/7	0	
	C666-1	Subcutaneous	8/8	0	
3	C666-1	tail vein	8/0	0	
	HONE-1	Nasopharynx	24/24	1	Lung
	C666-1	Nasopharynx	24/23	8	Bone (8), ovary, adrenal, kidney, liver (2)
4	C666-1	Nasopharynx (sirolimus)	18/15	0	
	C666-1	Nasopharynx (placebo)	18/16	6	Bone (2), lung (3), liver, colon
5	C666-1 #15	Nasopharynx	12/12	10	Bone (7), lung (7), ovary/uterus (3), liver, abdominal lymph node
6	C666-1 #15	Nasopharynx (placebo)	9/7	6	Bone (3), lung (3), ovary/uterus, peritoneal carcinomatosis
	C666-1#15	Nasopharynx (sirolimus)	9/9	3	Lung (3), ovary
Total	HONE-1	Nasopharynx	28/28	1 (3.6%)	
	C666-1	Nasopharynx	50/46	17 (40%)	

^aAll animals with metastatic tumors also have 1⁰ tumors.

^bThe numbers in parentheses represent the number of independently detected metastases. Some mice have more than one metastatic tumor.

Sirolimus disrupts metastasis. Having implicated differential regulation of the PI3K/AKT/mTOR axis in type III (undifferentiated) versus type II (differentiated) primary tumor biopsies, we hypothesized that this pathway directs the focally invasive and distant metastatic behavior of NPC *in vivo*. We selected the mTOR inhibitor, sirolimus, from the Connectivity Map data for *in vivo* experiments, and for orthotopic tumor cell inoculation, we again employed both the C666-1 or HONE-1 cell lines. Tumors were detected 18 to 21 days following injection, at which time the mice were randomized equally into sirolimus and placebo treatment groups. Treatment was maintained throughout the experiment. On average, growth of the primary C666-1 tumors was slowed by sirolimus, although the effect was modest (32% reduction; data not shown), and the focally invasive tumor features were preserved (Fig. 2A). By comparison, primary tumor growth in mice that received HONE-1 cells was unaffected (2% reduction; data not shown) by sirolimus. Thus, tumor growth at the primary site was not meaningfully inhibited by mTOR blockade.

Strikingly, however, growth of the metastatic lesions in C666-1 tumor-bearing mice was strongly attenuated. Shown graphically (Fig. 2B), metastatic lesions in the placebo-treated mice grew exponentially, while those treated with sirolimus were markedly slowed or eradicated. Specific examples are shown in Figure 2C and 2D. The placebo-treated mouse demonstrated unchecked exponential growth of the spine metastasis (Fig. 2C), whereas the femoral metastasis of the mouse treated with sirolimus dramatically

regressed (Fig. 2D). Thus, we have demonstrated that mTOR blockade affects metastatic but not primary-site NPC tumor growth in the xenograft model.

The finding of selective inhibition of metastatic tumor growth led us to speculate that an mTOR-mediated process directs tumor cell dissemination from the primary site and as such should be subject to modulation by sirolimus. To test this, 2 groups of mice were injected orthotopically with C666-1 cells ($n = 31$) (Table 1, experiment 4), and sirolimus treatment was started the day following tumor injection. The mice were assessed for the development of metastasis by routine live imaging for luciferase expression. Additionally, luciferin was injected just prior to sacrifice, which allowed extensive dissection and scanning of all internal organs for luciferase activity. In the treated group, there was no evidence of metastatic tumors in 15 of 15 mice ($P < 0.001$), although at the time they were sacrificed, they had a substantial primary tumor burden that was identical to that of the untreated group. By comparison, as expected, 6 of 16 (37.5%) in the untreated group developed metastases. Thus, dissemination from the primary tumor site that ultimately leads to metastatic tumor growth of the NPC C666-1 cells is an mTOR-dependent process that can be blocked by sirolimus.

Having shown that mTOR activity is necessary for the dissemination and metastatic growth of C666-1 tumors, we hypothesized that the metastatic C666-1 tumor cells have enhanced mTOR activity. To explore this, we removed metastatic C666-1 tumor cells from tumor-bearing mice and

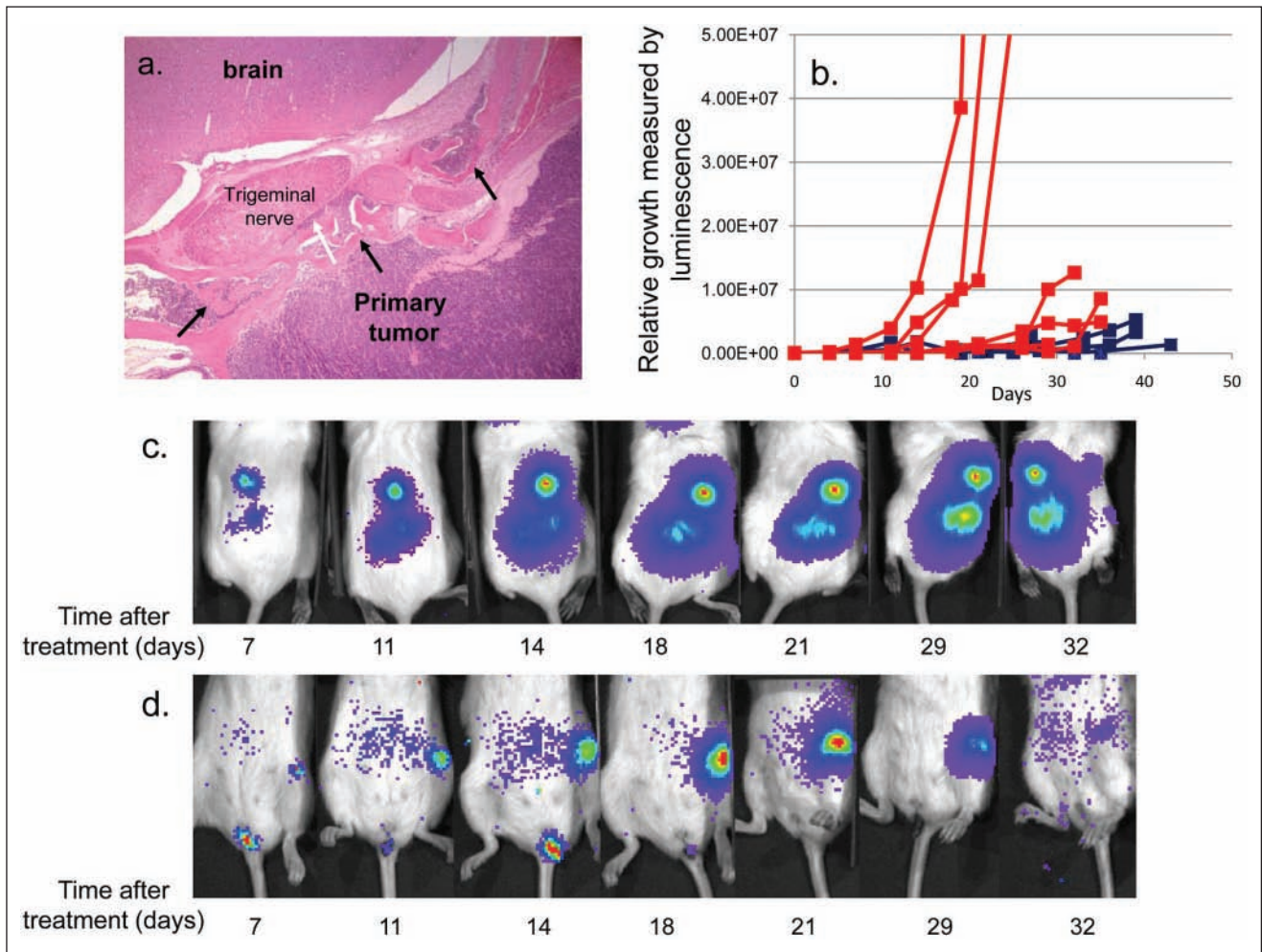


Figure 2. Sirolimus slows the growth of NPC metastasis. **(A)** H&E staining of a C666-1 primary-site tumor from a metastasis-bearing mouse that was treated with sirolimus and had regression of the metastatic tumor. Note bony invasion and remodeling (black arrows) as well as perineural invasion of the trigeminal nerve (white arrow). **(B)** Growth curves of multiple independent metastatic masses treated (blue, $n = 7$) or untreated (red, $n = 6$) with sirolimus immediately after tumors were detected, which was 18 ± 3 days after inoculation of tumor cells. Time 0 on the plot represents the time at which treatment with sirolimus or placebo was initiated. **(C)** A time series of viable animal scans, demonstrating growth of a metastatic tumor mass in the spine of a placebo-treated mouse, initiated 18 days after the inoculation of tumor cells. The time when scans were performed after the initiation of mock treatment is shown under each image. Note that the length of the scan varies according to the density of photon emission from the tumors, and therefore, the pictures cannot be used for quantitation of tumor growth. The actual quantitation derived from luciferase emission over time is shown in **(B)**. **(D)** As **(C)**, but for a mouse treated with sirolimus. Treatment was initiated 18 days after the inoculation of tumor cells. The x-axis indicates days after sirolimus treatment was started. Note that the mass has almost completely disappeared at the end of the time series.

expanded them in culture for comparison to the parental line. Two explants are described: one from a bone metastasis, no. 15, and the other from a liver metastasis, no. 7. Both were maintained in culture in a manner identical to that of the parental C666-1 line. As shown in Figure 3A to 3D, Western blot analysis confirms higher baseline mTOR activity by 3 parameters: 1) enhanced phosphorylation of 4E-BP1(Ser65), an indicator of mTOR complex 1 activity²⁵; 2) enhanced phosphorylation of Akt(Ser473), an indicator of mTOR complex 2 activity²⁶; and 3) higher baseline phosphorylation of mTOR(Ser2448), which is phosphorylated by mTOR complex 1 substrate, 70S6K,²⁷ and participates in both mTOR 1 and 2 complexes.²⁸

Because the metastatic tumor isolates maintain enhanced activation of mTOR in culture, we speculated that upon reinjection, they would metastasize more readily from the primary tumor site than the parental C666-1 counterpart. We chose subline no. 15 for further orthotopic xenograft experiments and found that 84% of xenograft recipients (compared to 40% of those injected with the parental; $P < 0.001$) developed metastases, many in multiple organs (Table 1, experiments 5 and 6). Thus, baseline up-regulation of mTOR activity in the C666-1 NPC line correlates with enhanced metastatic tumor behavior.

From this observation, we predicted that the more metastatic subline, shown to have higher baseline mTOR

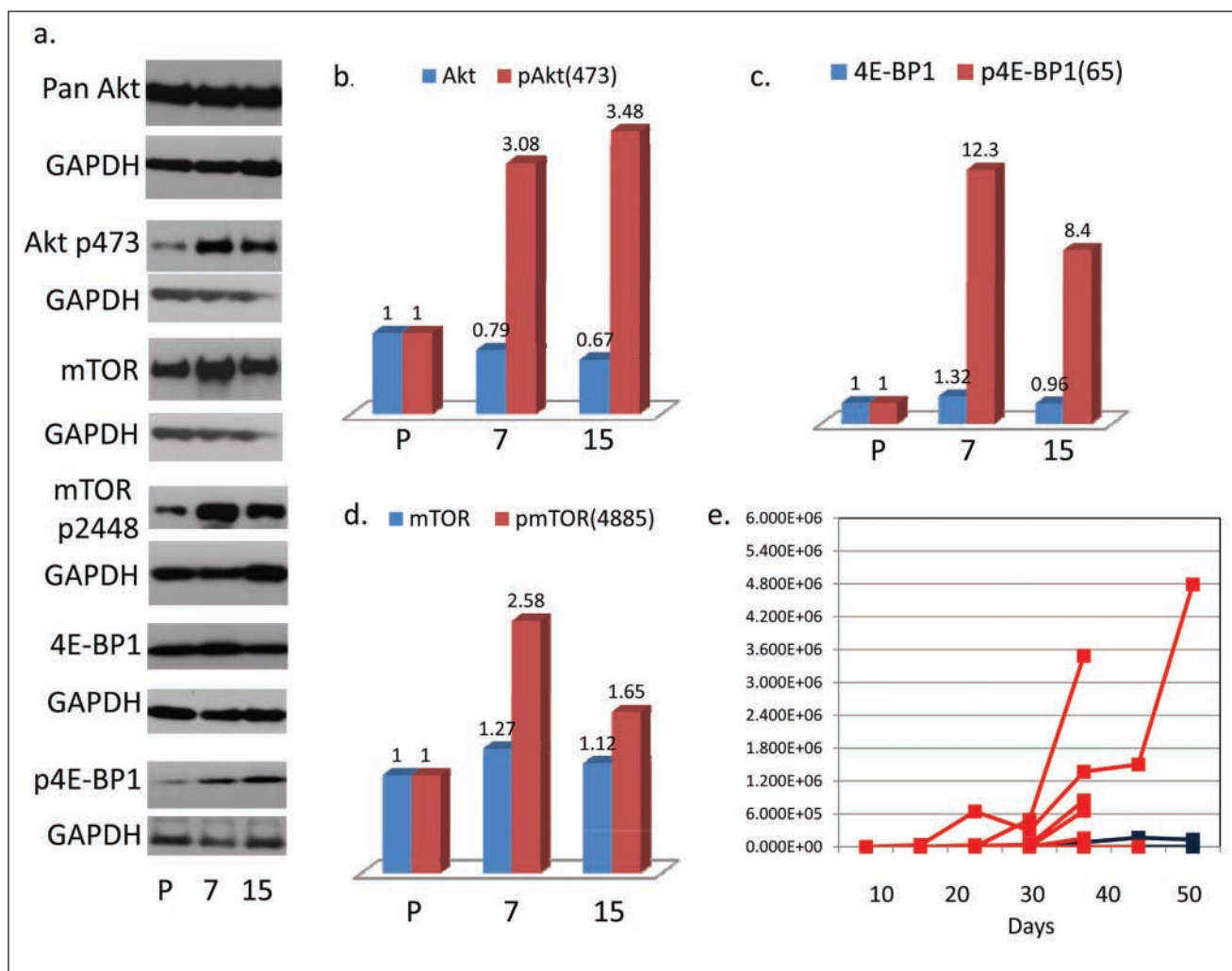


Figure 3. Metastatic explants have a higher baseline activation of mTOR based on phosphorylation levels of pAkt(473), pmTOR(4885), and p4E-BP1. Metastasis of explant no. 15 (from a bone lesion) is inhibited by sirolimus but demonstrates reduced sensitivity to sirolimus compared to the parental line. (A-D) Western blot analysis of metastatic explants: no. 15, bone metastasis, and no. 7, liver metastasis. The bar graphs describe fold increase of protein expression over the parental C666-1 line. (E) Growth curves of multiple independent metastases from mice injected with the metastatic C666-1 subclone, no. 15, treated with sirolimus (blue, $n = 3$) or placebo (red, $n = 6$) beginning the day following tumor injection. The x-axis indicates days after sirolimus treatment was started.

activity, would be less sensitive than the parental line to inhibition of metastasis by sirolimus. Following orthotopic placement of the highly metastatic C666-1 explant, no. 15, the mice were treated with sirolimus or placebo starting the day after injection (Table 1, experiment 6). Of the sirolimus treated, 3 of 9 with primary tumors developed metastatic disease compared to 6 of 7 that were treated with placebo ($P = 0.038$). As shown in Figure 3E, the metastatic burden was much greater in the placebo group, and in fact, the metastases in 2 of the 3 sirolimus-treated mice were very small lung tumors that could only be detected at the time of dissection. Thus, we demonstrate here that sirolimus does inhibit metastatic dissemination of the C666-1 explant, no. 15, but not to the extent that it inhibits dissemination of the parental C666-1 cells (Table 1, experiment 4, showing 0/15 mice with primary tumor–developed metastasis when

treated with sirolimus at the time of injection). This set of experiments supports the conclusion that metastatic C666-1 NPC cells have either acquired or been selected for dysregulated mTOR signaling, which potentiates enhanced dissemination to distant organs and, unlike the parental counterpart, is not fully overcome by mTOR blockade.

These studies suggest that differential activation of the mTOR pathway is instrumental in directing NPC tumor dissemination and that treatment with a targeted agent that blocks mTOR is effective for inhibiting NPC dissemination and metastatic growth.

Discussion

By developing a new orthotopic xenograft mouse model of nasopharyngeal carcinoma, we are able to recapitulate

patterns of human NPC invasion and metastasis that are useful for the study of tumor behavior and the development of antitumor therapies. We validated the utility of this method by demonstrating specific inhibition of metastatic growth via a targeted approach against mTOR, a key component of the PI3K/Akt/mTOR signaling pathway that is strongly implicated in metastasis across several tumor types.^{21,22}

Fundamental to this work is a detailed study of our orthotopic model to establish that it accurately recapitulates many aspects of advanced disseminated NPC. At the injection site, we saw a highly invasive tumor with skull base erosion, reactive bone formation, and invasion of cranial nerves. Although we do not persistently see cervical lymph node involvement, the model does replicate metastatic disease to multiple distant sites, including the bones, lungs, and liver, which are characteristics of advanced human disease²⁹ and are highly predictive of poor clinical outcome.^{30,31} Other reports describing xenograph models of NPC metastasis have not recapitulated the human disease as accurately.^{11,12} One study in particular described orthotopic injection of tumor cells into nude mice,¹¹ but we are unable to reproduce these results. In our hands, it was necessary to use highly immunodeficient NSG mice to see reproducible tumor growth and metastasis. The nude mouse study describes the use of a large gauge needle to inject cells directly through the hard palate, but in our experience, such injections caused massive tissue damage and disruption of surrounding tissues, including the base of the skull. Instead, we inject the cells into the soft tissue just distal and lateral to the hard palate with a small gauge needle, which allows us to obtain consistently reproducible focal tumor growth without collateral tissue damage. In the nude mouse study, metastasis was only observed in the brain, cervical lymph nodes, and lungs, a distribution that does not mimic the human disease. Specifically, metastasis to the brain is not a clinical characteristic of NPC,³² was not detected in our model, and may be accounted for in the nude mouse model by focal trauma caused by passing the needle through the hard palate. Thus, we have developed an orthotopic xenograft model of invasive and metastatic NPC disease that closely mimics human disease well enough to assist in further identifying cellular characteristics that direct aggressively invasive and disseminated growth as well as identifying effective targeted therapies.

The data shown in this particular study indicate that the dissemination and growth of metastatic cells that arise from a primary C666-1 tumor are highly dependent on mTOR activity. Specifically, sirolimus not only blocks C666-1 tumor cell dissemination to distant organs but also selectively inhibits their growth after metastasis has occurred. We further demonstrated that this is a feature of enhanced mTOR activation by showing that cultured metastatic explants maintain a higher baseline level of mTOR activation, which, upon

reinjection, renders the cells less sensitive to sirolimus and imparts a higher metastatic potential than the parental C666-1 counterpart. Interestingly, the enhanced mTOR activation of the metastatic explants found by Western blot analysis encompasses both mTOR complex 1 (TORC1) and complex 2 (TORC2) activity. Sirolimus is a rapalog compound that, as is characteristic of this class of drugs, is more active against TORC1 than TORC2. Its primary mechanism of action is understood to be dephosphorylation and consequent activation of eukaryotic translation initiation factor (eIF4E) binding proteins (4E-BP), which function to block eIF4E cap-dependent translation of mRNAs involved in cell growth and survival.³³ Indeed, the metastatic explants have a much higher baseline activation of 4E-BP1, consistent with its involvement in their metastatic behavior and our ability to affect this behavior by TORC1 inhibition. The role of enhanced TORC2 activity in the pathogenesis of C666-1 NPC tumor dissemination, however, is not specifically addressed by these studies. We speculate that more comprehensive mTOR inhibition may further diminish metastatic tumor development beyond what we observe with sirolimus. This can be readily investigated using the mouse model to study agents that inhibit both TORC1 and TORC2.

The results of our studies so far, however, indicate that targeting mTOR in NPC represents an approach of considerable clinical importance because there remains an urgent need for new therapeutic options for disseminated disease.³⁴ Current treatment protocols have resulted in very good clinical outcomes (currently 70% to 80% 3-year survival) if the cancer is diagnosed and treated while confined to locoregional areas.^{4,5,34} Metastatic NPC, however, is refractory to treatment and carries an extremely poor prognosis, with a median survival time of less than 12 months.^{5,35} Particularly concerning is, that among head and neck cancers of epithelial origin, NPC is associated with the highest rate of metastasis.⁶ Additionally, approximately half of recurrences are solid organ metastases,³⁶ which usually arise without nasopharyngeal site recurrence,¹⁴ suggestive of micrometastatic spread that arose prior to and was not ameliorated by treatment of the primary tumor. Thus, novel therapeutics such as mTOR inhibition, which specifically targets mechanisms that mediate dissemination, are essential to comprehensive NPC disease control. Moving forward, we can utilize our orthotopic model to refine mTOR inhibition strategies. As well, we can expand these strategies to include other components of the PI3K axis to develop clinically relevant interventions that will both prevent metastatic dissemination and effectively treat metastatic lesions.

Future studies should include commonly used chemotherapeutic agents for NPC, the prime example being cisplatin. Cisplatin resistance has been shown in a number of cancers, including NPC, to occur through up-regulation of Akt/mTOR,³⁷⁻³⁹ which we have shown here is linked to NPC metastasis. Furthermore, the EBV latent protein, LMP1, has

been shown to confer cisplatin resistance to the C666-1 NPC cell line in association with increased Akt activation.⁴⁰ Thus, cisplatin treatment may promote the development of a metastatic phenotype by selecting for resistance related to dysregulated mTOR activity. Our data raise the possibility that targeting mTOR, while treating with cisplatin, may prevent or reduce the development of chemotherapeutically resistant metastasis.

As an outgrowth of these explorations, we have gained some interesting preliminary insights into the pathophysiological differences between invasive and metastatic NPC. Following identification of the PI3K axis as a potential target through microarray analysis of primary biopsy type II and III specimens, we then demonstrated that mTOR activity directs metastatic dissemination in our orthotopic experimental model. Surprisingly, mTOR blockade did not change the local invasive characteristics of either cell line in the xenograft, even though the Connectivity Map analysis of the primary biopsy data indicates a correlation between higher activation of the PI3K/Akt/mTOR pathway and the more invasive features of the type III phenotype. This observation is consistent, however, with clinical studies. For example, PI3K amplification with consequent upregulation of Akt activity in primary NPC tumors has been shown to correlate with a poor prognosis resulting from higher rates of metastasis, irrespective of classification based on differentiation status.⁴¹ Similarly, enhanced rates of distant NPC metastasis have been shown to correlate with increased activation of mTOR and not the differentiation status of the primary tumors.⁴² Thus, we have more precisely defined a signaling pathway alteration that correlates with metastatic NPC behavior and confirmed that histological characteristics of focal invasion do not necessarily predict tumor dissemination to distant organs. Clarity regarding how the functions of focal cell invasion and distant metastatic dissemination are directed through the PI3K network will be gained through directed studies using drugs that specifically inhibit components of the pathway upstream of mTOR.⁴³ We anticipate that our orthotopic xenograft model, which clearly delineates these features of NPC tumor biology, will be ideal to conduct such studies.

Finally, we anticipate that our model will be useful to more directly interrogate the effects of EBV on invasive NPC pathogenesis. NPC tumors express a restricted pattern of EBV latent genes,⁴⁴ several of which have been suggested to play a role in NPC development, invasion, and metastasis.⁴⁴⁻⁴⁷ The orthotopic platform offers a valuable method by which we can more precisely delineate the effects of EBV transcription products on specific aspects of NPC tumor behavior *in vivo*.

Materials and Methods

Primary biopsy analysis. Total RNA was isolated from 20 fresh nonkeratinizing nasopharyngeal carcinoma biopsy

samples obtained from Taiwan.⁴⁸ Biopsy samples were obtained with punch forceps by use of endoscopic guidance. The tumor stage was designated according to the International Union Against Cancer and American Joint Committee on Cancer staging manuals (L.H. Sobin, 5th ed., 1997). NPCs were mostly of the advanced stage (IVA to IVC), and all samples were EBV positive as measured by EBER expression levels.⁴⁹

Biopsy material-chip hybridization. Biopsy RNA was isolated by guanidiniumthiocyanate extraction followed by centrifugation in CsCl, and RNA integrity was assessed by gel electrophoresis and optical density. We had sufficient RNA from 16 samples that also met the quality criteria for hybridization to Affymetrix microarray chips (HG-U95A, Santa Clara, CA). All scans were performed on Affymetrix scanners, and the expression value for each gene was calculated using Affymetrix GENECHIP software. A total of 14 samples survived the normalization and scaling criteria. For a detailed protocol and data set, see Pegtel *et al.*⁴⁸ and <http://www.broad.mit.edu/MPR/CNS>.

Computational analysis. The microarray data were normalized as previously described⁵⁰; details can be found at <http://www.broad.mit.edu>. We applied conventional marker selection techniques to this data set to identify and rank genes that were up- or down-regulated in type II versus type III NPC, based on fold change. We then used this gene profile to interrogate the Connectivity Map. The Connectivity Map¹⁸ (www.broadinstitute.org/cmap) is a database of gene expression profiles from cultured human cells treated with a large number of bioactive small molecules, many with multiple independent replicates, together with a pattern-matching tool that rank orders each treatment "instance" by its similarity to the query "signature" of interest (in our case, type III v. type II NPC gene array expression patterns).

Cell lines and transfectants. Cell lines were cultured with 10% heat-inactivated fetal bovine serum in either RPMI1640 (C666-1) or DMEM (HONE-1) at 37°C in 5% CO₂. C666-1 cells⁵¹ were obtained from Dr. Fei-Fei Liu (Ontario Cancer Institute, Toronto, Canada) and HONE-1⁵² from Dr. Ron Glaser, who originated the line (Ohio State University, Columbus, OH). Both lines retain expression of human cytokeratins, and C666-1 harbors the Epstein-Barr virus. Luciferase was expressed in the cells from the pGL4.51 (luc2.CMV/Neo) vector (Promega, Fitchburg, WI) introduced by electroporation with the BTX High Throughput Electroporator (model HT-200, BTX). Alternatively, cells were infected with the pGreenFire1-CMV, TR011VA-1 lentivirus (System Biosciences, Mountain View, CA).

Tumor injection and imaging. The highly immunodeficient mouse strain NOD.Cg-Prkdc^{scid} Il2rg^{tm1Wjl}/SzJ (NSG) was used in all experiments. Mice were maintained and treated

according to institutional guidelines of the Tufts University Division of Laboratory Animal Medicine, and the experimental techniques described herein were approved by the Tufts University Institutional Animal Care and Use Committee (protocol #56-08). For nasopharyngeal injections, mice were subject to deep anesthesia with ketamine/xylazine (100 mg/kg and 10 mg/kg) and placed in a prone position with the mouth held open with curved forceps and the tongue pulled aside. Cells (2.5×10^5 cells in 30 μ L of PBS) were injected using a 25-gauge needle just distal and lateral to the hard palate. For subcutaneous growth, 5×10^5 tumor cells in 100 μ L of PBS were injected into the subcutis of the right flank. For tail vein inoculation, 2×10^5 cells were injected in a total volume of 300 μ L of PBS. Tumor appearance was detected and/or growth measured, every 4 to 7 days, by IP administration of luciferin (1 mg in 100 μ L of PBS). The mice were immobilized with isoflurane anesthesia and imaged in a Xenogen IVIS 200 Biophotonic Imager, Xenogen. Final numerical representations of tumor size were calculated by determining photon emission/second of a given tumor within a radius encompassing 5% or greater of maximal signal intensity.

Sirolimus administration. Sirolimus (10 mg/mL) (LKT Laboratories, St. Paul, MN) stored at -20°C in 100% ethanol was diluted into PBS containing 5% PEG300 and 5% Tween80, for a final dose of 5 mg/kg in 100 μ L. Placebo-treated mice received PBS/PEG300/Tween80 only. Drug was administered IP for 5 of every 7 days.

Histology. Histological analysis was performed by the Clinical Histology laboratory or the Department of Laboratory Animal Medicine at Tufts Medical Center using a Ventana Benchmark XT automated system, Ventana. Tumor tissue and metastases were excised from sacrificed mice, employing luciferase imaging to identify the tissue of interest. For cytokeratin staining, the AE1/AE3/PCK26 anti-pancytokeratin antibody was used (Ventana), and for EBER *in situ* hybridization, the INFORM EBER Probe (Ventana) was used.

Western blot analyses. Western blotting was performed using primary antibodies against Akt (pan) (C67E7, rabbit mAb #4691S, Cell Signaling Technology, Danvers, MA), phospho-Akt (Ser473) (rabbit mAb #4060S, Cell Signaling Technology), mTOR (7C10, rabbit mAb #2983S, Cell Signaling Technology), phospho-mTOR (Ser2448) (rabbit mAb #2971S, Cell Signaling Technology), 4E-BP1 (53H11) (rabbit mAb #9644S, Cell Signaling Technology), phospho-4E-BP1 (Thr37/46) (236B4, rabbit mAb #2855S, Cell Signaling Technology), and GAPDH (14C10, #2118S, Cell Signaling Technology). The secondary antibody was HRP-linked anti-rabbit IgG (#7074, Cell Signaling Technology),

and the blots were developed using Super Signal* West Femto Chemiluminescent Substrate (#34095, Thermo Scientific, Waltham, MA).

Acknowledgments

The authors thank Jennifer Bradford for technical assistance with developing the nasopharyngeal tumor injection technique, Justin Lamb for introducing us to the Connectivity Map, Evan Smith for assistance in developing Western blotting protocols, and Lauren Richey for interpretation of pathology slides.

Declaration of Conflicting Interests

The author(s) declared no potential conflicts of interest with respect to the research, authorship, and/or publication of this article.

Funding

The author(s) received the following financial support for the research, authorship, and/or publication of this article: This work was supported by Public Health Service grants R01 CA65883, R01 AI18757, and R01 AI062989 to D.A.T.-L.

References

1. Parkin DM, Muir CS. Cancer incidence in five continents: comparability and quality of data. *IARC Sci Publ.* 1992;(120):45-173.
2. Ayadi W, Khabir A, Hadhri-Guiga B, *et al.* [North African and Southeast Asian nasopharyngeal carcinomas: between the resemblance and the dissemblance]. *Bull Cancer.* 2010;97(4):475-82.
3. Toumi N, Frikha M, Siala W, *et al.* [Juvenile nasopharyngeal carcinoma: anatomoclinic, biologic, therapeutic and evolutive aspects]. *Bull Cancer.* 2010;97(4):427-33.
4. Lee AW, Sze WM, Au JS, *et al.* Treatment results for nasopharyngeal carcinoma in the modern era: the Hong Kong experience. *Int J Radiat Oncol Biol Phys.* 2005;61(4):1107-16.
5. O'Sullivan B. Nasopharynx cancer: therapeutic value of chemoradiotherapy. *Int J Radiat Oncol Biol Phys.* 2007;69(2 Suppl):S118-21.
6. Skinner DW, Van Hasselt CA, Tsao SY. Nasopharyngeal carcinoma: modes of presentation. *Ann Otol Rhinol Laryngol.* 1991;100(7):544-51.
7. Gullo C, Low WK, Teoh G. Association of Epstein-Barr virus with nasopharyngeal carcinoma and current status of development of cancer-derived cell lines. *Ann Acad Med Singapore.* 2008;37(9):769-77.
8. Hui AB, Yue S, Shi W, *et al.* Therapeutic efficacy of seliciclib in combination with ionizing radiation for human nasopharyngeal carcinoma. *Clin Cancer Res.* 2009;15(11):3716-24.
9. Kato H, Ito E, Shi W, *et al.* Efficacy of combining GMX1777 with radiation therapy for human head and neck carcinoma. *Clin Cancer Res.* 2010;16(3):898-911.
10. Ke X, Yang YC, Hong SL. EBV-LMP1-targeted DNase restrains nasopharyngeal carcinoma growth in a mouse C666-1 xenograft model. *Med Oncol.* 2011;28(Suppl 1):S326-32.
11. Liu T, Ding Y, Xie W, *et al.* An imageable metastatic treatment model of nasopharyngeal carcinoma. *Clin Cancer Res.* 2007;13(13):3960-7.

12. Lum CT, Liu X, Sun RW, *et al.* Gold(III) porphyrin 1a inhibited nasopharyngeal carcinoma metastasis in vivo and inhibited cell migration and invasion in vitro. *Cancer Lett.* 2010;294(2):159-66.
13. Dubrulle F, Souillard R, Hermans R. Extension patterns of nasopharyngeal carcinoma. *Eur Radiol.* 2007;17(10):2622-30.
14. Teo PM, Kwan WH, Lee WY, Leung SF, Johnson PJ. Prognosticators determining survival subsequent to distant metastasis from nasopharyngeal carcinoma. *Cancer.* 1996;77(12):2423-31.
15. Sham JS, Cheung YK, Chan FL, Choy D. Nasopharyngeal carcinoma: pattern of skeletal metastases. *Br J Radiol.* 1990;63(747):202-5.
16. Nicholls JM. Nasopharyngeal carcinoma: classification and histologic appearances. *Adv Anat Pathol.* 1997;4(2):71-84.
17. Lamb J. The Connectivity Map: a new tool for biomedical research. *Nat Rev Cancer.* 2007;7(1):54-60.
18. Lamb J, Crawford ED, Peck D, *et al.* The Connectivity Map: using gene-expression signatures to connect small molecules, genes, and disease. *Science.* 2006;313(5795):1929-35.
19. Hennessy BT, Smith DL, Ram PT, Lu Y, Mills GB. Exploiting the PI3K/AKT pathway for cancer drug discovery. *Nat Rev Drug Discov.* 2005;4(12):988-1004.
20. Larue L, Bellacosa A. Epithelial-mesenchymal transition in development and cancer: role of phosphatidylinositol 3' kinase/AKT pathways. *Oncogene.* 2005;24(50):7443-54.
21. Sabatini DM. mTOR and cancer: insights into a complex relationship. *Nat Rev Cancer.* 2006;6(9):729-34.
22. Weinberg RA. Mechanisms of malignant progression. *Carcinogenesis.* 2008;29(6):1092-5.
23. Cui C, Liu L, Ma J, *et al.* Trigeminal nerve palsy in nasopharyngeal carcinoma: correlation between clinical findings and magnetic resonance imaging. *Head Neck.* 2009;31(6):822-8.
24. Kim EK, Yun SJ, Ha JM, *et al.* Selective activation of Akt1 by mammalian target of rapamycin complex 2 regulates cancer cell migration, invasion, and metastasis. *Oncogene.* 2011;30(26):2954-63.
25. Graff JR, Konicek BW, Carter JH, Marcusson EG. Targeting the eukaryotic translation initiation factor 4E for cancer therapy. *Cancer Res.* 2008;68(3):631-4.
26. Sarbassov DD, Guertin DA, Ali SM, Sabatini DM. Phosphorylation and regulation of Akt/PKB by the rictor-mTOR complex. *Science.* 2005;307(5712):1098-101.
27. Chiang GG, Abraham RT. Phosphorylation of mammalian target of rapamycin (mTOR) at Ser-2448 is mediated by p70S6 kinase. *J Biol Chem.* 2005;280(27):25485-90.
28. Rosner M, Siegel N, Valli A, Fuchs C, Hengstschlager M. mTOR phosphorylated at S2448 binds to raptor and rictor. *Amino Acids.* 2010;38(1):223-8.
29. Sham JS, Cheung YK, Choy D, Chan FL, Leong L. Nasopharyngeal carcinoma: CT evaluation of patterns of tumor spread. *AJNR Am J Neuroradiol.* 1991;12(2):265-70.
30. Cheng SH, Jian JJ, Tsai SY, *et al.* Long-term survival of nasopharyngeal carcinoma following concomitant radiotherapy and chemotherapy. *Int J Radiat Oncol Biol Phys.* 2000;48(5):1323-30.
31. Yamashita S, Kondo M, Hashimoto S. Squamous cell carcinoma of the nasopharynx: an analysis of failure patterns after radiation therapy. *Acta Radiol Oncol.* 1985;24(4):315-20.
32. Cvitkovic E, Bachouchi M, Boussen H, *et al.* Leukemoid reaction, bone marrow invasion, fever of unknown origin, and metastatic pattern in the natural history of advanced undifferentiated carcinoma of nasopharyngeal type: a review of 255 consecutive cases. *J Clin Oncol.* 1993;11(12):2434-42.
33. Ma XM, Blenis J. Molecular mechanisms of mTOR-mediated translational control. *Nat Rev Mol Cell Biol.* 2009;10(5):307-18.
34. Razak AR, Siu LL, Liu FF, Ito E, O'Sullivan B, Chan K. Nasopharyngeal carcinoma: the next challenges. *Eur J Cancer.* 2010;46(11):1967-78.
35. Kwong DL, Sham JS, Au GK, *et al.* Concurrent and adjuvant chemotherapy for nasopharyngeal carcinoma: a factorial study. *J Clin Oncol.* 2004;22(13):2643-53.
36. Geara FB, Sanguineti G, Tucker SL, *et al.* Carcinoma of the nasopharynx treated by radiotherapy alone: determinants of distant metastasis and survival. *Radiother Oncol.* 1997;43(1):53-61.
37. Ma BB, Lui VW, Hui EP, *et al.* The activity of mTOR inhibitor RAD001 (everolimus) in nasopharyngeal carcinoma and cisplatin-resistant cell lines. *Invest New Drugs.* 2010;28(4):413-20.
38. Liu LZ, Zhou XD, Qian G, Shi X, Fang J, Jiang BH. AKT1 amplification regulates cisplatin resistance in human lung cancer cells through the mammalian target of rapamycin/p70S6K1 pathway. *Cancer Res.* 2007;67(13):6325-32.
39. Peng DJ, Wang J, Zhou JY, Wu GS. Role of the Akt/mTOR survival pathway in cisplatin resistance in ovarian cancer cells. *Biochem Biophys Res Commun.* 2010;394(3):600-5.
40. Mei YP, Zhou JM, Wang Y, *et al.* Silencing of LMP1 induces cell cycle arrest and enhances chemosensitivity through inhibition of AKT signaling pathway in EBV-positive nasopharyngeal carcinoma cells. *Cell Cycle.* 2007;6(11):1379-85.
41. Fendri A, Khabir A, Mnejja W, *et al.* PIK3CA amplification is predictive of poor prognosis in Tunisian patients with nasopharyngeal carcinoma. *Cancer Sci.* 2009;100(11):2034-9.
42. Chen J, Hu CF, Hou JH, *et al.* Epstein-Barr virus encoded latent membrane protein 1 regulates mTOR signaling pathway genes which predict poor prognosis of nasopharyngeal carcinoma. *J Transl Med.* 2010;8:30.
43. Fasolo A, Sessa C. Current and future directions in mammalian target of rapamycin inhibitors development. *Expert Opin Investig Drugs.* 2011;20(3):381-94.
44. Shah KM, Young LS. Epstein-Barr virus and carcinogenesis: beyond Burkitt's lymphoma. *Clin Microbiol Infect.* 2009;15(11):982-8.
45. Moody CA, Scott RS, Amirghahari N, *et al.* Modulation of the cell growth regulator mTOR by Epstein-Barr virus-encoded LMP2A. *J Virol.* 2005;79(9):5499-506.
46. Scholle F, Bendt KM, Raab-Traub N. Epstein-Barr virus LMP2A transforms epithelial cells, inhibits cell differentiation, and activates Akt. *J Virol.* 2000;74(22):10681-9.
47. Shair KH, Schnegg CI, Raab-Traub N. Epstein-Barr virus latent membrane protein-1 effects on junctional plakoglobin and induction of a cadherin switch. *Cancer Res.* 2009;69(14):5734-42.
48. Pegtel DM, Subramanian A, Sheen TS, Tsai CH, Golub TR, Thorley-Lawson DA. Epstein-Barr-virus-encoded LMP2A induces primary

- epithelial cell migration and invasion: possible role in nasopharyngeal carcinoma metastasis. *J Virol.* 2005;79:15430-42.
49. Hochberg D, Souza T, Catalina M, Sullivan JL, Luzuriaga K, Thorley-Lawson DA. Acute infection with Epstein-Barr virus targets and overwhelms the peripheral memory B-cell compartment with resting, latently infected cells. *J Virol.* 2004;78(10):5194-204.
 50. Pomeroy SL, Tamayo P, Gaasenbeek M, *et al.* Prediction of central nervous system embryonal tumour outcome based on gene expression. *Nature.* 2002;415(6870):436-42.
 51. Cheung ST, Huang DP, Hui AB, *et al.* Nasopharyngeal carcinoma cell line (C666-1) consistently harbouring Epstein-Barr virus. *Int J Cancer.* 1999;83(1):121-6.
 52. Glaser R, Zhang HY, Yao KT, *et al.* Two epithelial tumor cell lines (HNE-1 and HONE-1) latently infected with Epstein-Barr virus that were derived from nasopharyngeal carcinomas. *Proc Natl Acad Sci U S A.* 1989;86(23):9524-8.